

Development of a Numerical Model for the Formation of Complete and Incomplete Channel Blockages and Their Influences on River Flow

Takashi Wada^{1*}, Hiroshi Miwa¹, Naoto Aoki¹, Yusei Fujii²

¹Department of Social Systems and Civil Engineering, Tottori University, Tottori, JAPAN

²Aisawa Construction Co., Ltd., Okayama, JAPAN

*Corresponding author: wada-t@tottori-u.ac.jp

SUBMITTED 31 December 2024 REVISED 18 March 2025 ACCEPTED 20 March 2025

ABSTRACT Large landslides, triggered by torrential rain or earthquakes, can slide down mountainous slopes and block river channels at the lower end of the slopes. In cases where the landslide volume is relatively small compared to the river discharge, or when the distance between the landslide slope and the river channel is long, incomplete channel blockages may occur due to an insufficient supply of landslide material to fully block the river flow. Since the shape of the channel blockage is the final result obtained through the temporal changes in landslide material movement, river flow, and topography, considering their interactions, it is necessary to investigate the blockage shape by numerical analysis that accounts for these interactions. Therefore, we developed a numerical model to predict the formation of various channel blockages by incorporating the combined conditions of topography, landslide volume, and river discharge. The developed model is a two-dimensional (2-D) model, which can connect several one-dimensional calculation areas for mountainous streams at any selected point in the 2-D area. In addition, the model can consider landslide material movements represented by cylindrical blocks. To verify our model and identify appropriate values for the associated parameters, we investigated the MAE (mean absolute error) for the deposit thickness distribution and the PWO (percentage of the area where the actual and calculated waterlogged areas overlapped) between the actual and calculated results using our model for two previous channel blockages of different sizes. Although our model and the associated parameters still need to be improved by considering the loss of landslide material, they are useful for estimating the magnitude and area of damage caused by large-scale landslides and the associated channel blockage and waterlogging in various river channels with steep side slopes. The calculated results can be utilized in investigating disaster countermeasures for landslides in the area.

KEYWORDS Numerical modeling; Two-dimensional calculation; Channel blockage; River flow; Landslide material movement.

© The Author(s) 2025. This article is distributed under a Creative Commons Attribution-ShareAlike 4.0 International license.

1 INTRODUCTION

In East and Southeast Asia, including Japan, large-scale landslides triggered by torrential rains or earthquakes can occur on mountainous slopes, causing landslide materials to block river channels at the lower end of the slopes (Hung, 2000; Sassa, 2005; Li et al., 2011; Fan et al., 2012; Ishizuka et al., 2017; Van Tien et al., 2018). Blocked river flow on the upstream side of the blockages can lead to flooding of buildings in waterlogged areas, while on the downstream side, debris flows caused by erosion due to overflow from the blockages can result in severe flood damage. Thus, channel blockages (landslide dams) may lead to multimodal sediment disasters on both the upstream and downstream sides.

A complete blockage does not necessarily occur due to the inflow of landslide material into a river channel. For example, the river channel blockage in Hsiaolin Village, Taiwan, caused by heavy rainfall from Typhoon Morakot in 2008, was formed by the inflow of large-scale landslide material. However, the blockage quickly failed due to the erosion by overtopping floodwater resulting from the large river flood discharge (Li et al., 2011). A similar case occurred during the 2011 heavy

rainfall disaster on the Kii Peninsula in Japan. Heavy rainfall from Typhoon Talas triggered multiple large-scale landslides, and more than half of the channel blockages failed to fully block the river. Consequently, these blockages collapsed within a day of formation (Inoue and Doshida, 2012). There were many cases where a complete blockage did not occur due to insufficient landslide material reaching the river channel. According to the database by Peng and Zhang, which includes 1,239 landslide dams worldwide, 87% of the 204 recorded landslide dams with failure data collapsed within a year, 71% within a month, 51% within a week, and 34% within a day (Peng and Zhang, 2012).

The formation of river blockages, whether complete or incomplete, depends on the relationship between the volume of landslide material flowing into the river and the river's channel size (or flow discharge). Additionally, the volume of landslide material is affected by the topographic conditions between the landslide slope and the river channel, through sedimentation and other processes. In the 2011 Kii Peninsula disaster, the incomplete blockages may have occurred be-

cause the channel width and river discharge were large enough that the supplied landslide volume was insufficient to fully block the river flow. Chen et al. (2019) also suggested that in-channel deposition of landslide material inflowing into the channel, which leads to landslide dam formation, is affected by the channel width and flow depth. Therefore, it is essential to develop a method to predict the types of river channel blockages, such as complete or incomplete, under various conditions, considering the topography and river characteristics, to implement effective countermeasures for each type of blockage.

Previous studies have primarily focused on damage estimation downstream of landslide dams caused by floods resulting from dam failures. Several statistical analyses have been conducted to predict the magnitude of dam-break floods (e.g., peak flow rate, hydrographs) based on dam shape parameters (such as height, volume, and impounded water volume). These studies proposed various relational equations to describe the relationship between dam shape and dam-break floods (Costa, 1985; Walder and O'Connor, 1997; Chen et al., 2019; Fan et al., 2020). Additionally, numerous studies have investigated the failure processes of landslide dams using numerical simulations (e.g., Takahashi and Kuang (1988); Takahashi and Nakagawa (1993); Awal et al. (2008); Akazawa et al. (2014); Takayama et al. (2021); Zhong et al. (2024)), laboratory experiments (e.g., Takahashi and Kuang (1988); Takahashi and Nakagawa (1993); Awal et al. (2008); Zhou et al. (2019)), and field experiments (e.g., Akazawa et al. (2014); Zhong et al. (2019); Takayama et al. (2021)) to identify the characteristics of floods caused by dam failures. These studies have elucidated the process of landslide dam destruction by dividing it into several patterns.

The above research indicates that the flood hydrograph caused by landslide dam failure is strongly related to the dam shape. Therefore, understanding the dam shape formation process is important. However, few studies have focused on the formation process of channel blockages (landslide dam formation) resulting from the inflow of landslide material into a river channel. Swanson et al. (1986) and Costa and Schuster (1988) proposed a geomorphological classification method based on the channel topography, which identifies where channel blockages may form. However, this method is a statistical classification based on target topographic conditions and does not clarify how topography contributes to the formation process or final shape of the blockage. Liao et al. (2019) conducted flume experiments to examine the kinematic processes and emplacement of rockslides, and the factors that dictate landslide dam formation. Their experimental results suggest that the height and shape of landslide dams, such as incomplete or complete blockages, are influenced by rockslide volume, rock fragmentation, and river flow depth. Crosta et al. (2003) proposed contin-

uum finite element models consisting of the conservation equations of mass, momentum, and energy for rock and debris avalanches caused by landslides. However, this is a model for flow-like landslides in vertical two-dimensions, and it is difficult to account for the influence of planar topography. In addition, their model did not consider the dam formation processes in conjunction with river flow. Since the shape of a channel blockage is the final result obtained through temporal changes in landslide material movement, river flow, and topography, considering their interactions, it is necessary to investigate the blockage shape by numerical analysis that includes these interactions.

In this study, we aimed to establish a prediction method for the formation process of river channel blockages due to the inflow of landslide materials into a river channel, under various combinations of topography, landslide volume, and river discharge. Our objective was achieved by developing a planar two-dimensional (2-D) numerical flow model with cylindrical blocks representing landslide material. We validated the developed model and its associated parameters by comparing the simulated results with actual blockage formation and expanded flood areas.

2 DEVELOPED NUMERICAL MODEL

Figure 1 provides an overview of the developed model and its base model. The developed model is based on the two-dimensional model “Numerical Model Considering Multiple Inflows of Debris Flows and River Floods” by Wada et al. (2021), which predicts inundation volume and area caused by the simultaneous occurrence of debris flows and river floods. In the model, the downstream ends of several 1-D calculation areas for mountain streams are connected to a 2-D calculation area for the floodplain at any selected point. We incorporated into the model, the landslide material movements represented by cylindrical blocks, as developed by Satofuka and Takahashi (2003). Thus, the model can simultaneously predict multiple flows, flood propagation processes, and landslide material movement. This indicates that the model can predict how landslide material inflowing into flood flows changes the flow direction, resulting in river blockage formation on a two-dimensional plane.

2.1 1-D and 2-D flow calculation parts

Figure 2 shows the outlines of the 1-D and 2-D calculation parts of the developed model. Several 1-D calculation areas are integrated into a unified temporary 1-D calculation area, separated by designated calculation points at the upstream ends ($i_{st,n}$, n : number of 1-D calculation areas) and downstream ends ($i_{e,n}$), for each 1-D area. These 1-D areas operate indepen-

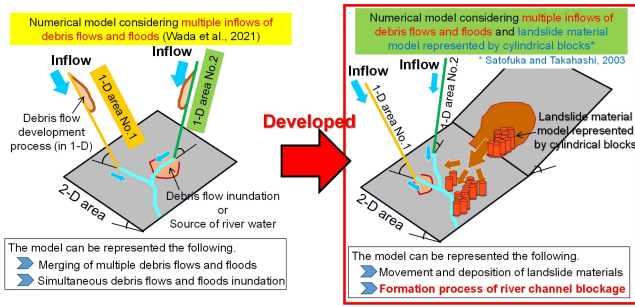


Figure 1 Outlines of the developed model (left) and its base model (right)

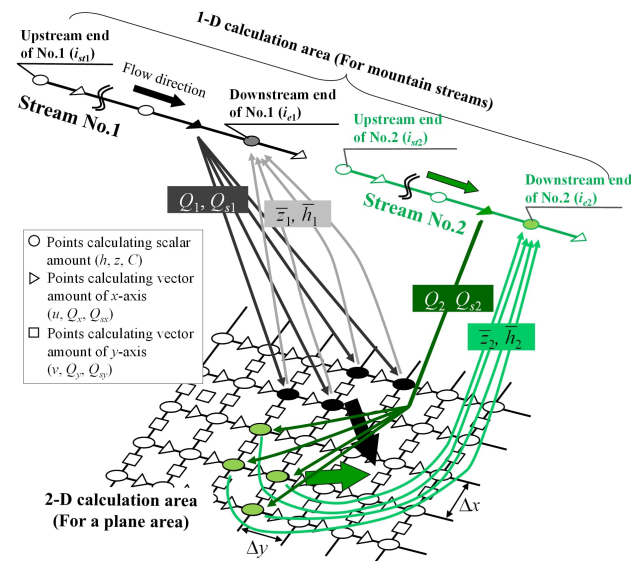


Figure 2 Outline of base model for our developed model. (Partially revised the figure by Wada et al. (2021))

dently. The model applies several 1-D and 2-D models at each time step. In addition, the discharge (Q_n) and the sediment discharge (Q_{bn}) from the debris flow at the downstream ends of the 1-D Areas are added to the inflow point in the 2-D calculation area. The average bed elevation (z_{ave_n}) and flow depth (h_{ave_n}) at the inflow points are assigned to the bed elevation and flow depth at the downstream ends of the 1-D areas. The transfer of momentum from the 1-D areas to the 2-D area is also considered in the model. The model enables continuous calculation of debris flows and river floods on multiple streams, including their inflows into stream and river confluences, and the resulting deposition and flood propagation. For calculation point placement, staggered grids are used in the model. Specifically, vector quantity calculation points are placed $1/2\Delta x$ or $1/2\Delta y$ downstream (positive directions of the x -axis or y -axis directions) from the scalar calculation points, where Δx and Δy represent the grid spacing along x - and y -axes in the 2-D area. For further details on the connection between the 1-D and 2-D areas in the model, please refer to Wada et al. (2021).

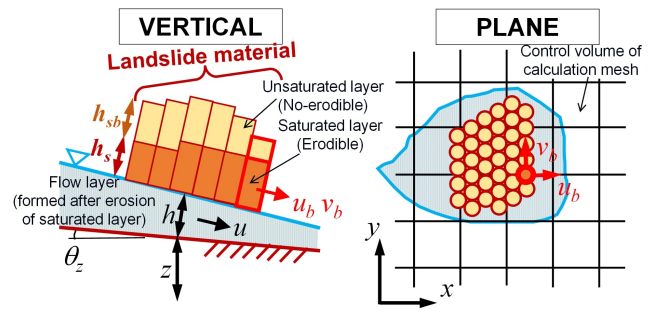


Figure 3 Outline of landslide material models represented by cylindrical blocks. (Quoted from Satofuka and Takahashi (2003)).

2.2 Landslide cylindrical block model

Figure 3 illustrates the landslide material model represented by cylindrical blocks. The landslide material is considered an assembly of vertically standing circular cylinders arranged in a hexagonal close-packed structure. To account for porosity between the cylinders, when a hexagonal column is converted into a cylindrical block, the cylinder diameter is increased so that the cross-sectional area matches that of the original hexagonal column.

The block shape is cylindrical to allow consistent calculation of distances between block surfaces in all directions. However, a disadvantage is that converting the landslide material into cylindrical blocks creates gaps between blocks that do not exist in reality. This disadvantage can be mitigated by optimally setting the parameters related to the soil properties of the block.

A cylindrical block consists of an upper unsaturated layer and a lower saturated layer; only the saturated layer can be eroded by bottom friction. At the bottom of the cylinder, the eroded saturated layer is transformed into a debris flow with a sediment concentration of 0.5, while the remaining landslide material is carried on the surface of the block. The water content required for debris flow formation is supplied by the remaining cylindrical blocks. When the movement velocity of a cylindrical block is sufficiently low (i.e., below the threshold velocity for stopping block movement, U_{blim}), the landslide material is considered deposited, and the volume of the remaining block is transferred into a rising riverbed volume at the stopping point.

The cylindrical blocks move due to surface topographic irregularities and interactions with other blocks. Each block is affected by gravity and frictional forces acting on its bottom along the slope direction, based on surrounding topographic irregularities. Additionally, the block is influenced by soil cohesion and repulsive forces that prevent overlap with neighboring blocks. These forces depend on the distance between blocks and their relative movement direction. When a flow layer is present beneath a block, shear forces based

on velocity differences between the block and the flow layer also affect the block. These forces are introduced for modeling convenience, and their physical validity should be verified in future studies.

2.3 Governing equations

2.3.1 Equations for a cylindrical block and its motion

A cylindrical block is composed of a lower saturated layer (saturation ratio: S_b) and an upper unsaturated layer, with thicknesses of h_s and h_{sb} , respectively, as illustrated on the left side of Figure 2. The mass of a block (M_b) is given by:

$$M_b = \rho_T S_0 (\alpha_1 h_{sb} + h_s) \quad (1)$$

where S_0 is the bottom area of a block, ρ_T is the apparent density of the saturated layer, and α_1 is the difference in density between the saturated and unsaturated layers, which is expressed as:

$$\alpha_1 = \frac{\rho_{Tb}}{\rho_T} = \frac{\sigma C_{*T} + \rho(1 - C_{*T})S_b}{\sigma C_{*T} + \rho(1 - C_{*T})} \quad (2)$$

where ρ_{Tb} is the apparent density of the unsaturated layer, and C_{*T} is the volume concentration of sediment in the static mass.

The x - and y -direction equations for the migration velocities of a block (u_b, v_b) are as follows:

$$\frac{\partial U_b}{\partial t} = g \sin\theta_{hx} + \frac{\tau_{sx} S_0}{M_b} + \frac{1}{M_b} (\Sigma f_x + \Sigma f_{sx}) \quad (3)$$

$$\frac{\partial v_b}{\partial t} = g \sin\theta_{hy} + \frac{\tau_{sy} S_0}{M_b} + \frac{1}{M_b} (\Sigma f_y + \Sigma f_{sy}) \quad (4)$$

where t is the time; g is the gravitational acceleration; θ_{hx} and θ_{hy} are the x - and y -direction gradients of the flow layer's surface (if no flow layer exists, they represent the gradients of the bed surface), τ_{sx} and τ_{sy} are the x - and y -direction boundary shear stresses, respectively, f_x and f_y are the x - and y -direction cohesion or repulsive forces between blocks around it, respectively, f_{sx} and f_{sy} are the x - and y -direction shear stress fractions between blocks around it, and Σ is the summation of these forces. The soil cohesion force (c_b) determines the values of $f_x, f_y, f_{sx},$ and f_{sy} . The overlapping area ratio for the bottom of the k -th block and the calculation mesh at point (I, j) , denoted as $(P_{k(I,j)})$ is used to determine the forces acting on each block. For further details on the calculation of these forces, please refer to Satofuka and Takahashi (2003) and Takahashi (2007).

2.3.2 Governing equations for debris and flood flows including the flow layer below a block bottom

The governing equations for debris and flood flows, erosion/deposition, and riverbed shear stress were partially modified from the equations used in the previous debris flow simulation by Nakagawa et al. (1996). The following are the governing equations for the 2-D area. The equations for the 1-D area are derived by excluding the y -direction terms. In the 1-D area, longitudinal changes in stream width can be considered using averaged hydraulic quantities in the cross-stream direction. Note, however, that energy loss in debris flows due to rapid width changes cannot be strictly accounted for in a 1-D area.

The continuity equation for the total volume of debris flow is:

$$\frac{\partial h}{\partial t} + \frac{\partial M}{\partial x} + \frac{\partial N}{\partial y} = i + i_b \quad (5)$$

where h is the flow depth, M and N are the momentum fluxes in the x - and y -directions ($M = u_h, N = v_h$), respectively, u and v are the flow velocities in the x - and y -directions, respectively, I is the erosion/deposition rate of the riverbed, and i_b is the erosion rate of a cylindrical block supplied from its bottom. I_b is based on the physical properties of landslide material, which are insufficiently understood. For convenience, the following formula was used to determine the i_b value of each cylindrical block:

$$i_b = \frac{S_0}{\Delta x \Delta y} \beta \sqrt{(u - u_b)^2 + (v - v_b)^2} \quad (6)$$

where β is a coefficient related to the erosion rate at the bottom of the cylindrical block. Although β was 0.012 in the previous simulation for flow and deposition caused by a past large-scale landslide (Satofuka, 2004), the value was identified through trial-and-error in this study.

The continuity equation for the volume of sediment in a debris flow is:

$$\frac{\partial Ch}{\partial t} + \frac{\partial CM}{\partial x} + \frac{\partial CN}{\partial y} = iC_* + i_b C_{*T} \quad (7)$$

where C is the sediment concentration in the debris flow, and C_* is the sediment concentration in the initial mobile layer of the riverbed.

The momentum equation in the x -direction is:

$$\frac{\partial M}{\partial t} + \frac{\partial uM}{\partial x} + \frac{\partial vM}{\partial y} = -gh \frac{\partial H}{\partial x} - \frac{\tau_{bx}}{\rho'} - \frac{\tau_{sx}}{\rho'} \quad (8)$$

where H is the flow surface level ($H = z + h$), z is the riverbed level, τ_{bx} is the riverbed shear stress in the x -direction, and ρ' is the apparent mass density of the

debris flow ($= \tau \times C + \rho_m \times (1-C)$), τ is the mass density of the sediment, and ρ_m is the mass density of the interstitial fluid).

The momentum equation in the y -direction is:

$$\frac{\partial N}{\partial t} + \frac{\partial uN}{\partial x} + \frac{\partial vN}{\partial y} = -gh \frac{\partial H}{\partial y} - \frac{\tau_{by}}{\rho'} - \frac{\tau_{sy}}{\rho'} \quad (9)$$

where τ_{by} is the riverbed shear stress of the y -direction.

The continuity equation for the riverbed level is:

$$\frac{\partial z}{\partial t} + i = 0 \quad (10)$$

The bed shear stresses (τ_{bx}, τ_{by}) are calculated using three different flow resistance theories based on sediment-transport modes: debris flow, sediment sheet flow, and ordinary turbulent water flow including bed material load. These flow modes are classified according to the sediment concentration of the debris flow I . The erosion/deposition rate of the riverbed (i) depends on the large/small relationship between C and the equilibrium sediment concentration (C_∞). If C is smaller than C_∞ , the erosion rate is positive value ($i_b > 0$), meaning the flow erodes the riverbed. Conversely, if C is larger than C_∞ , the deposition occurs ($i_b < 0$). C_∞ is calculated by using the equations proposed by Takahashi (1991). For further details on the above equations, please refer to Takahashi (1991).

The finite-difference method was used to discretize these equations in the model. Forward, upwind, and centered finite-difference methods were used for time discretization, the discretization of advective terms, and spatial discretization, respectively.

Table 1. Topographic and geologic conditions in both landslide disasters

Contents	Obara landslide	Ichinose landslide
Landslide volume	30,000 m ³	330,000 m ³
Distance between the landslides slope and river channel	~45 m	~150 m
Landslide-slope inclination	~24°	~30°
Inclination between the landslides slope and river channel	~8°	~22°
Dimensionless net resistance coefficient, 1/R	3.48	1.51
Estimated river discharges	36.74 m ³ s ⁻¹ *	133.245 m ³ s ⁻¹ **
Geologic properties	Weathered granite	Pelitic schist

* The coefficient was equal to L/H, where L is the horizontal distance from landslide source to deposit area, and H is the vertical elevation of the source above the area, proposed by Iverson (1997).

** The value was estimated by the rational formula using the actual hourly rainfall intensity at near observation point.

*** Value corresponds to the actual daily average river discharge at a neighboring observation station.

3 REPRODUCTION CALCULATION FOR VALIDATION OF DEVELOPED MODEL

3.1 Target river blockages by inflowing landslides

The targets for reproduction calculations using the developed model were two landslides of different scales: the landslide in the Obara district, Hyogo Prefecture, in 2018, with a volume of 30,000 m³ (quoted in the investigation report of The Japan Landslide Society, 2018), and the landslide in the Ichinose district, Tottori Prefecture, in 2004, with a volume of 330,000 m³ (quoted in The Japan Landslide Society, 2013). Figures 4 and 5 show the outlines of the target landslides, respectively.

The topographic and geologic conditions in the two districts are different, as shown in Table 1. In particular, the distances and inclinations between the landslide slopes and river channels are remarkably different. In addition, the dimensionless net resistance coefficients proposed by Iverson (1997), L/H , in both districts are also different, with $L/H > 2$ in the Obara district and $L/H < 2$ in the Ichinose district. Based on his experimental results with well-sorted gravel, the landslide material in Obara could have been unsaturated, whereas the material in Ichinose may have been saturated. Despite these differences, both landslides

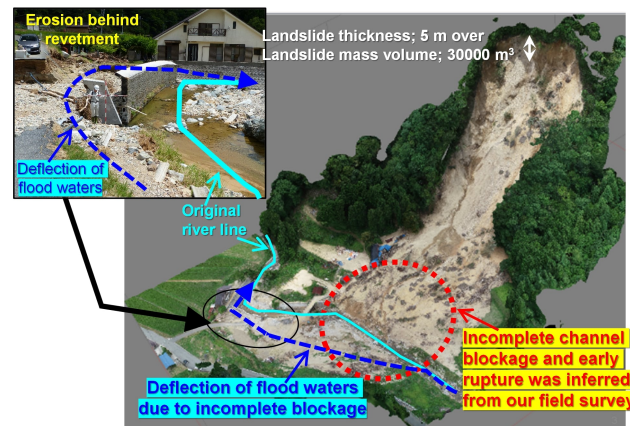


Figure 4 Landslide disaster and short-term river blockage in the Obara district, Hyogo Prefecture

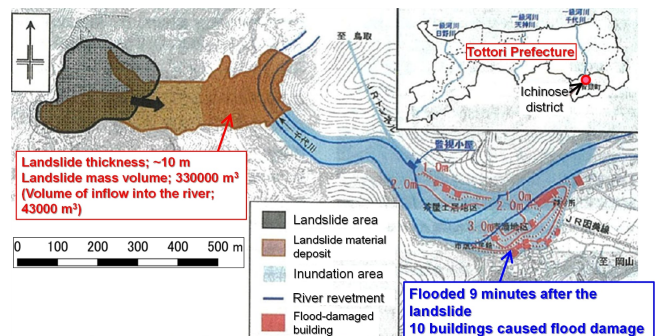


Figure 5 Area for validation of calculation result and identification of optimal values in Ichinose district

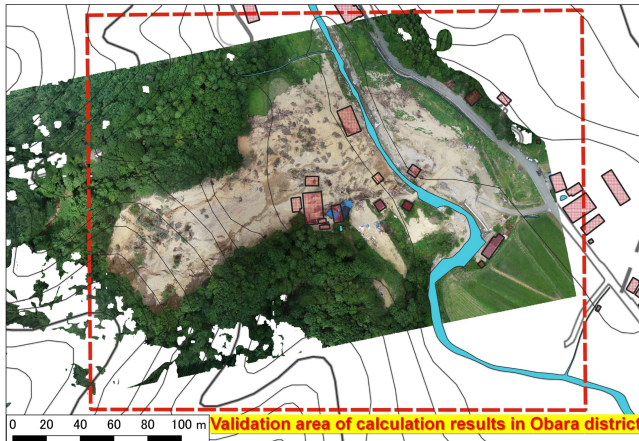


Figure 6 Landslide disaster and river blockage in the Ichinose district, Tottori Prefecture. (quoted from The Japan Landslide Society, 2013)

blocked the river channels at the lower end of the slope.

In the former case (Obara), as illustrated in Figure 4, the blockage was not confirmed in subsequent field investigations. We suggest that the landslide material supplied to the river was insufficient to maintain the blockage, leading to its early disappearance. As shown in Figure 4, the temporary blockage caused a change in flood flow direction, diverting the main flow behind the revetment on the opposite bank, which led to erosion at the rear of the revetment. In contrast, the magnitude of the latter landslide (Ichinose) was large enough to completely block river flow at the base of the slope. On the upstream side, the river overflowed due to retained floodwater, resulting in inundation of several riverside buildings. After the landslide occurred, a spillway tunnel was constructed through the opposite side of the mountain to release the accumulated floodwater caused by the river channel blockage.

3.2 Calculation condition

The calculations involved multiple cases with different combinations of values for three parameters: the coefficient of block bottom erosion, β , the cohesion of the landslide cylinder block, c_b , and the threshold velocity for stopping block movement, U_{blim} . These parameters remain physically unclear, and their values were varied within ranges close to those proposed by Satofuka (2004). Table 2 lists the parameters used in the reproduction calculations. For the Obara landslide, appropriate parameter values were identified to best reproduce the actual deposit thickness distribution. The method for validating and identifying optimal parameter values is described in the next section. These identified values were then used as a reference to define parameter ranges for the reproduction calculation of the larger Ichinose landslide.

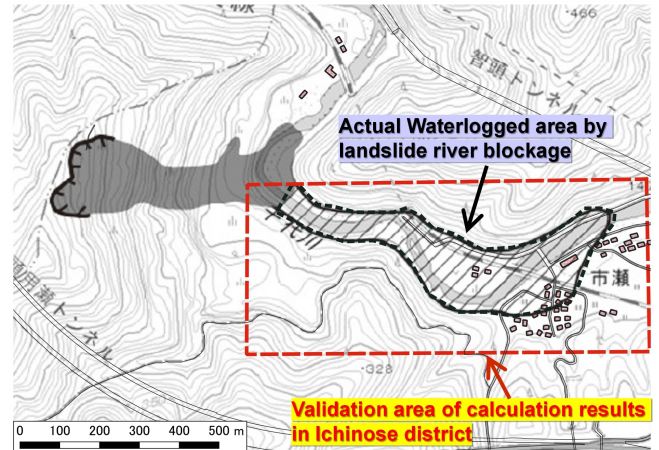


Figure 7 Area for validation of calculation results and identification of optimal values in the Obara district

3.3 Verification and Identification for optimal parameter values

To verify the calculation results and identify optimal parameter values in the Obara case, we evaluated the Mean Absolute Error (MAE) between actual and calculated deposit thicknesses in each case. The parameter set that yielded the lowest MAE was considered optimal. MAE is calculated using the following equation:

$$MAE = \frac{1}{N} \sum_{i=1}^N |dz_{ical} - dz_{isur}| \quad (11)$$

where N is the total number of 2-D calculation points in the validation area shown in Figure 6, i is the number of the calculation point, dz_{ical} is the calculated deposit thickness at the i th-point, and dz_{isur} is the corresponding surveyed value.

In the Ichinose case, validation and parameter optimization were conducted by calculating the Percentage of Waterlogged Overlap (PWO), defined as the proportion of the actual waterlogged area correctly predicted by the simulation. The validation area is shown in Figure 7.

$$PWO = \frac{n_{wlap}}{n_{wlap} + n_{wact_only} + n_{wcal_only}} \quad (12)$$

where n_{wlap} is the number of the calculation points whose calculated flood depths are larger than 0.05 m within the actual waterlogged area shown in Figure 5, n_{wact_only} is the number of the points whose calculated flood depths are smaller than 0.05 m within the actual waterlogged area, and n_{wcal_only} is the number of the points whose calculated flood depths are larger than 0.05 m without the actual waterlogged area.

Table 2. Parameters incorporated in reproduction calculations

Parameters/Variables	Value of landslide		Unit
	Obara	Ichinose	
Total simulation time (T_{max})		10800	s
Time step (Δt)		0.01	s
Minimum flow depth of flux (h_{fmin})		0.05	m
Minimum flow depth (h_{min})		0.01	m
Manning's roughness coefficient (n_m)		0.03	$m^{-1/3} s$
Gravity acceleration (g)		9.8	$m s^{-2}$
Diameter of sediment (d^*)		0.005	m
Volume density of sediment (s^*)		2650	$kg m^{-3}$
Volume density of interstitial fluid (r^*)		1000	$kg m$
Sediment concentration by volume in the movable bed layer (C^*)		0.65	-
Internal friction angle of sediment ($tan\phi^*$)		0.75	-
Coefficient of erosion rate (δe^*)		0.0007	-
Coefficient of deposition rate (δd^*)		0.05	-
Diameter of sediment (d^*)		0.005	m
River flow discharge (Constant supply)	36.74	133.245	$m^3 s^{-1}$
Total landslide volume (Including internal void)	30000	330000	m^3
Landslide cylinder model size	A regular hexagon with 2 m on each side		-
Number of cylinder model	548	4886	-
Time of Starting landslide movement	1 hour after starting of calculation		-
Cohesion (c_b) **	0.05, 0.10, 0.20, 0.50	0.05, 0.10, 0.15	$kN m^{-2}$
Coefficient of bottom erosion (b) **	0.010, 0.050, 0.100	0.010, 0.050	-
Threshold velocity for stopping movement (U_{blim}) **	0.05, 0.50	0.50	-
Saturation in lower unsaturated layer		0.30	-
Coefficient of dynamic bottom friction, Generating debris flow at the bottom		0.30	-
No debris flow at the bottom		0.50	-
Number of 2-D calculation points ($i_{e2} \times j_{e2}$)	156 \times 183	906 \times 464	-
Interval of 2-D calculation points ($D_{x2} \times D_{y2}$)	2 \times 2		m

* Values referenced from the debris flow simulation by Nakagawa et al. (1996).

** These parameters were varied across multiple calculation cases.

4 CALCULATION RESULTS AND DISCUSSION

4.1 Identification of appropriate coefficient of bottom erosion (β)

The appropriate β value was investigated by comparing the actual and calculated landslide deposit thickness distributions in the Obara district. Figure 8 presents the actual and calculated results for the deposit thickness distribution in cases where only the β value differs, while c_b and U_{lim} values had common values of $100 N m^{-2}$ and $0.50 m s^{-1}$, respectively. The figure shows that when β is 0.05 or 0.10, the calculated results closely align with the actual landslide thickness distribution. If β is significantly less than 0.05, the calculated deposition area becomes larger than the actual area, which is not considered $\beta < 0.05$ was appropriate. The MAEs for the deposit thickness distribution in cases where β were 0.01, 0.05, and 0.10 were 1.137,

1.075, and 0.839, respectively. These suggested that the appropriate β value to predict the landslide sediment movement accurately was the value range from 0.05 to 0.10, and closer to 0.10. This value is larger than the $\beta = 0.012$ used in the previous simulation by Satofuka (2004), possibly reflecting the fact that the landslide material in this case was more easily decomposed due to heavy weathering. This may also be influenced by the unsaturated condition of the material, as suggested by Iverson's coefficient L/H , indicating that landslides involving unsaturated materials may have higher erosion coefficients.

4.2 Identification of appropriate cohesion of cylindrical block (c_b)

The appropriate c_b value was investigated using the same approach as in Section 4.1. Figure 9 shows the

actual and calculated results for the deposit thickness distribution in cases where only c_b differs, while β and U_{lim} were fixed at 0.05 and 0.50 m s⁻¹, respectively. The calculated results under $c_b = 50$ or 100 N m⁻² agree relatively well with the actual thickness distribution. However, when c_b was increased to 200 N m⁻², the calculated deposition area was smaller than the actual one, resulting in poorer reproducibility. The MAEs in cases where c_b were 50, 100, and 200 N m⁻² were 1.026, 1.075, and 1.302, respectively. This suggested that the appropriate c_b value was the value range from 50 to 100 N m⁻².

The appropriate c_b value was also investigated in terms of the calculated river-flow distributions in these cases. Figure 10 depicts the calculated flow-depth distribution two hours after the landslide. The results under $c_b = 50$ or 100 N m⁻² well predicted the partial river blockage by inflowing the landslide material. Additionally, these results also predicted the changes of the main flow direction, passing behind the opposite-side revetment. This also suggested that the appropriate c_b value was the value range from 50 to 100 N m⁻². Note that these calculated river blockages remained two hours af-

ter the landslide. Further investigation is needed to determine whether this blockage could be cleared by overtopping flow using extended calculation periods.

The estimated appropriate c_b value was slightly smaller than the value of 179 N m⁻² set in the previous simulation by Satofuka (2004). This may suggest that the landslide material was easily decomposed due to the great weathering. This value is an order of magnitude (10⁻¹) less than that of general physical soil properties. This discrepancy might be attributed to the consolidation of finer landslide material particles into virtual larger blocks in the model. The difference between actual and modeled c_b values should be further explored in future studies.

4.3 Identification of appropriate threshold velocity for stopping movement (U_{blim})

The appropriate U_{blim} value was also investigated in the same manner of 4.1 and 4.2. Figure 11 presents the actual and calculated results for the landslide deposit thickness distribution in cases where only U_{blim} varies, with β and c_b fixed at 0.05 and 100 N m⁻². The figure illustrates that the differences between the results for

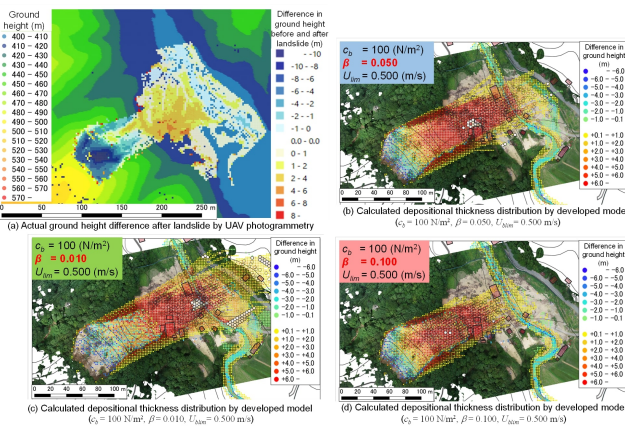


Figure 8 Calculated results for deposit thickness distribution two hours after the landslide in the Obara district, showing cases where only the coefficient of bottom erosion (β) differs

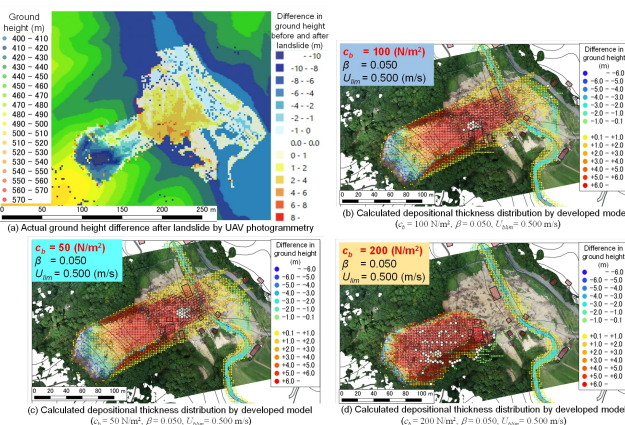


Figure 9 Calculated results for deposit thickness distribution 2 h after the landslide in the Obara district, showing cases where only cohesion of landslide cylindrical block (c_b) differs

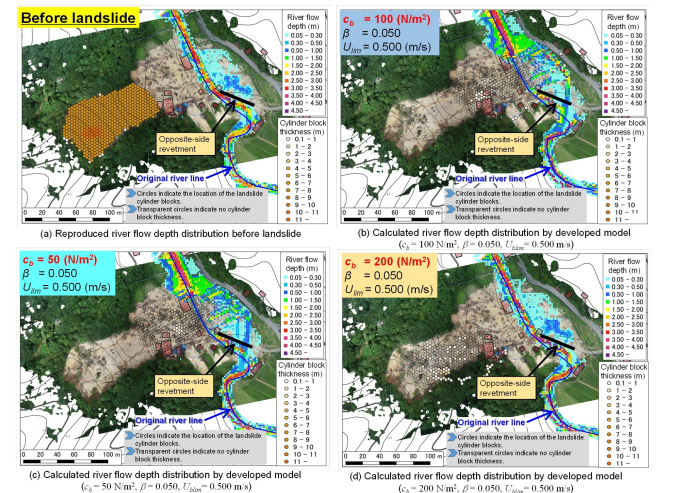


Figure 10 Calculated results for river flow depth distribution 2 h after the landslide in the Obara district, showing cases where only cohesion of landslide cylindrical block (c_b) differs

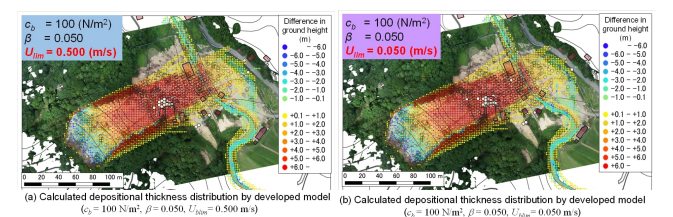


Figure 11 Calculated results for deposit thickness distribution 2 h after the landslide in the Obara district, showing cases where only threshold velocity for stopping block movement (U_{blim}) differs

Table 3. MAEs of actual and calculated results for the deposit thickness distribution in each case

Parameter values			
Coefficient of bottom erosion (β)	Cohesion of cylinder block (c_b) ($N\ m^{-2}$)	Threshold velocity for stopping movement (U_{blim}) ($m\ s^{-1}$)	MAE
0.01	50	0.50	1.208
	100	0.05	1.148
	200	0.50	1.137
	500	0.50	1.031
0.05	50	0.50	1.026
	100	0.05	1.072
	200	0.50	1.075
	500	0.50	0.935
0.10	50	0.50	0.797
	100	0.05	0.836
	200	0.50	0.839
	500	0.50	1.030

Table 4. PWOs of actual and calculated results for the deposit thickness distribution in each case

Parameter values			
Coefficient of bottom erosion (β)	Cohesion of cylinder block (c_b) ($N\ m^{-2}$)	Threshold velocity for stopping movement (U_{blim}) ($m\ s^{-1}$)	PWO
0.01	50		0.617
	100	0.50	0.569
	150		0.475
0.05	50		0.436
	100	0.50	0.436
	150		0.437
0.10	50		0.437
	100	0.50	0.437
	150		0.437

cases where only U_{blim} differs are slight. The MAEs in cases where U_{blim} were 0.05 and 0.50 $m\ s^{-1}$ were almost identical at 1.072 and 1.075, respectively. Thus, U_{blim} exhibits a minimal effect on the deposit distribution. This suggested that the decomposition of the front-part material was completed before the cylindrical blocks stopped moving.

4.4 Identification for optimal parameter values of Obara's landslide

We investigated all MAEs of the actual and calculated results under all combinations for β , c_b , U_{blim} as shown in Table 3. The optimal parameter values, that is the case with the smallest MAE is under the combination for $\beta = 0.10$, $c_b = 50\ N\ m^{-2}$, $U_{blim} = 0.50\ m\ s^{-1}$.

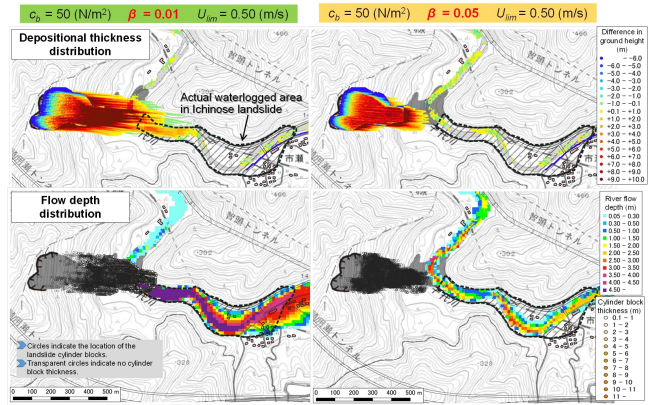


Figure 12 Calculated results for distributions of deposit thickness and river flow depth 1 h after the landslide in Ichinose district for $\beta = 0.01$ or 0.05, in cases where c_b and U_{blim} values had common

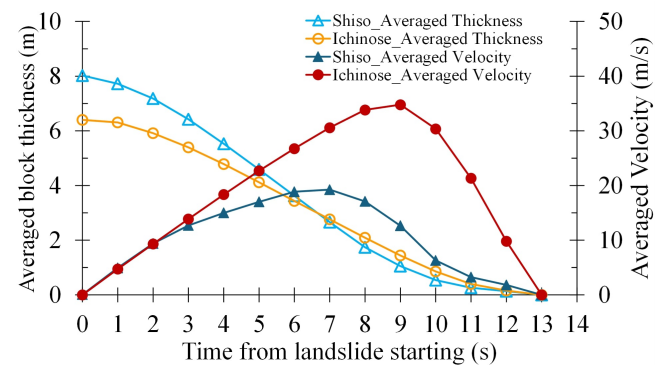


Figure 13 Temporal variation of block-averaged thicknesses and movement velocities for both landslide calculations under the combination for $\beta = 0.01$, $c_b = 50\ N\ m^{-2}$, $U_{blim} = 0.50\ m\ s^{-1}$

4.5 Identification for optimal parameter values of Ichinose's landslide

We investigated all PWOs by comparing the actual and calculated waterlogged areas caused by the Ichinose landslide under all combinations of β , c_b , U_{blim} as shown in Table 4. The table shows that the appropriate β and c_b values for accurately predicting the Ichinose landslide movement were approximately 0.01, and 50 $N\ m^{-2}$, respectively. In all cases where β was greater than or equal to 0.05, the PWO was less than 0.45; PWO < 0.45 indicates that only river flow occurred, without waterlogging caused by a river channel blockage. The appropriate β value for the Ichinose landslide was much smaller than that for the Obara landslide. This difference may reflect that the degree of weathering affected block bottom erosion during movement. Considering that the Ichinose landslide material could have been saturated, as suggested by Iverson's coefficient, L/H , the saturation of the landslide material may have also contributed to lower erosion coefficients. Investigating the loss mechanisms of landslide materials during movement is necessary, particularly by considering their physical properties, such as particle size distribution, weathering, and water content.

Figure 12 displays the distributions of landslide deposit thickness and river flow depth one hour after the landslide in the Ichinose district for cases where only the β value differs, while c_b and U_{blim} were fixed at 50 N m^{-2} and 0.50 m s^{-1} , respectively. In the case where $\beta = 0.05$, the landslide material did not reach the river channel, and consequently, waterlogging did not occur. The case with $\beta = 0.01$ produced results closer to the actual inundation damage. However, the calculated results only partially matched the observed areas of landslide deposition and waterlogging. This discrepancy is attributed to a decrease in the volume of cylindrical blocks caused solely by bottom erosion during their movement. According to Figure 13, which shows the temporal variation of block-averaged thicknesses and movement velocities for both landslide cases under the combination of $\beta = 0.01$, $c_b = 50 \text{ N m}^{-2}$, and $U_{blim} = 0.50 \text{ m s}^{-1}$, the velocities of the Obara landslide were lower than those of the Ichinose landslide due to its milder slope inclination. However, the erosion rates of the blocks in both cases were similar, with erosion being completed in approximately the same amount of time. This suggests that the developed model needs to incorporate additional processes for block decomposition, such as soil dispersal.

5 CONCLUSION

We developed a numerical model to predict the formation of various channel blockages by incorporating combined conditions of topography, landslide volume, and river discharge. The model successfully reproduced two landslides, of different scales and their impacts on river flows by optimizing the soil-related parameters of the cylindrical block model. Although the simulated river blockage in Obara persisted for two hours, post-disaster surveys showed it had already disappeared. Further investigation is needed to determine whether the blockage could have been cleared by overtopping flows during an extended simulation period.

The appropriate c_b and U_{blim} values for both landslides were the same, which were 50 N m^{-2} and 0.50 m s^{-1} , respectively. The c_b value is an order of magnitude (10^{-1}) less than that of general physical soil properties. The difference between actual and modeled c_b values should be further explored in future studies. The appropriate β value for the Ichinose's landslide was much smaller than that for the Obara's landslide. The results suggest that the difference for weathering progress and saturation of both landslide materials effect on the loss of the block during their movement. These findings indicate that the loss of landslide material is influenced not only by bottom erosion and material fluidization but also by additional mechanisms related to their physical property, such as particle size distribution, weathering, and water content, such as soil dispersion. To enhance the accuracy of the model in predict-

ing various channel-blockage formations, future studies should focus on investigating the transport mechanisms of the landslide materials, incorporating a wider range of values for these physical factors.

Although the developed model still needs to be improved in identification of optimal β value and consideration of the loss of landslide material, it is useful for estimating the magnitude and area of damage caused by a large-scale landslide and the associated channel blockage and waterlogging in various river channels with their side steep slopes. The calculated results can be utilized in investigating disaster countermeasures for the landslide in the area.

DISCLAIMER

The authors declare no conflict of interest.

ACKNOWLEDGMENTS

This study was supported by a Research Grant by Sabo and Landslide Technical Center (STC).

REFERENCES

- Akazawa, F., Ikeda, A., Hayami, S., Harada, N., Satofuka, Y., Miyata, S. and Tsutsumi, D. (2014), 'Numerical simulation of landslide dam deformation by overtopping flow', *International Journal of Erosion Control Engineering* 7(3), 85–91.
URL: <https://doi.org/10.13101/ijece.7.85>
- Awal, R., Nakagawa, H., Kawaike, K., Baba, Y. and Zhang, H. (2008), 'An integrated approach to predict outflow hydrograph due to landslide dam failure by overtopping and sliding', *Proceeding of Hydraulic Engineering* 52, 151–156.
URL: <https://doi.org/10.2208/prohe.52.151>
- Chen, K. T., Chen, X. Q., Hu, G. S., Kuo, Y. S., Huang, Y. R. and Shieh, C. L. (2019), 'Dimensionless assessment method of landslide dam formation caused by tributary debris flow events', *Geofluids*, 7083058.
URL: <https://doi.org/10.1155/2019/7083058>
- Costa, J. E. (1985), Floods from dam failures, Open-File Report 85-560, US Geological Survey.
URL: <https://doi.org/10.3133/ofr85560>
- Costa, J. E. and Schuster, R. L. (1988), 'The formation and failure of natural dams', *Geological Society of America Bulletin* 100(7), 1054–1068.
URL: [https://doi.org/10.1130/0016-7606\(1988\)100<1054:TFAFON>2.3.CO;2](https://doi.org/10.1130/0016-7606(1988)100<1054:TFAFON>2.3.CO;2)
- Crosta, G. B., Imposimato, S. and Roddeman, D. G. (2003), 'Numerical modelling of large landslides stabil-

ity and runout', *Natural Hazards and Earth System Sciences* **3**, 523–538.

URL: <https://doi.org/10.5194/nhess-3-523-2003>

Fan, X., Dufresne, A., Subramanian, S. S., Strom, A., Hermanns, R., Stefanelli, C. T., Hewitt, K., Yunus, A. P., Dunning, S., Capra, L., Geertsema, M., Miller, B., Casagli, N., Jansen, J. D. and Xu, Q. (2020), 'The formation and impact of landslide dams – state of the art', *Earth-Science Reviews* **203**, 103116.

URL: <https://doi.org/10.1016/j.earscirev.2020.103116>

Fan, X., van Westen, C. J., Xu, Q., Gorum, T. and Dai, F. C. (2012), 'Analysis of landslide dams induced by the 2008 wenchuan earthquake', *Journal of Asian Earth Sciences* **57**, 25–37.

URL: <https://doi.org/10.1016/j.jseaes.2012.06.002>

Hung, J. J. (2000), 'Chi-chi earthquake induced landslides in taiwan', *Earthquake Engineering and Engineering Seismology* **2**(2), 25–32.

Inoue, K. and Doshida, S. (2012), 'Comparison of distribution of disasters occurring in 1889 and 2011 on kii peninsula', *Journal of Japan Society of Erosion Control Engineering* **65**(3), 42–46. In Japanese with English abstract.

URL: https://doi.org/10.11475/sabo.65.3_42

Ishizuka, T., Kaji, A., Morita, K. and Mizuyama, T. (2017), 'Analysis for a landslide dam outburst flood in ambon island, indonesia', *International Journal of Erosion Control Engineering* **10**(1), 32–38.

URL: <https://doi.org/10.13101/ijece.10.32>

Iverson, R. M. (1997), 'The physics of debris flows', *Reviews of Geophysics* **35**(3), 245–296.

URL: <https://doi.org/10.1029/97RG00426>

Li, M., Sung, R., Dong, J., Lee, C. and Chen, C. (2011), 'The formation and breaching of a short-lived landslide dam at hsiaolin village, taiwan - part ii: Simulation of debris flow with landslide dam breach', *Engineering Geology* **123**(1–2), 60–71.

URL: <https://doi.org/10.1016/j.enggeo.2011.05.002>

Liao, H., Yang, X., Lu, G., Tao, J. and Zhou, J. (2019), 'Experimental study on the river blockage and landslide dam formation induced by rock slides', *Engineering Geology* **261**, 105269.

URL: <https://doi.org/10.1016/j.enggeo.2019.105269>

Nakagawa, H., Takahashi, T., Sawada, T. and Satofuka, Y. (1996), 'Design hydrograph and evacuation planning for debris flow', *Annual Report of Disaster Prevention Research Institute, Kyoto University* **39**(B-2), 347–371. In Japanese with English abstract.

Peng, M. and Zhang, L. M. (2012), 'Breaching parameters of landslide dams', *Landslides* **9**(1), 13–31.

URL: <https://doi.org/10.1007/s10346-011-0271-y>

Sassa, K. (2005), 'Landslide disasters triggered by the 2004 mid-niigata prefecture earthquake in japan', *Landslides* **2**(2), 135–142.

URL: <https://doi.org/10.1007/s10346-005-0054-4>

Satofuka, Y. (2004), 'Numerical simulation of the debris flow at the atsumari river, minamata city, 2003', *Annual Journal of Hydraulic Engineering* **48**, 925–930. In Japanese with English abstract.

URL: <https://doi.org/10.2208/prohe.48.925>

Satofuka, Y. and Takahashi, T. (2003), 'Numerical simulation of a debris flow caused by landslide', *Annual Journal of Hydraulic Engineering* **47**, 583–588. In Japanese with English abstract.

URL: <https://doi.org/10.2208/prohe.47.583>

Swanson, F. J., Oyagi, N. and Tominaga, M. (1986), Landslide dams in japan, in 'Proceedings of Landslide Dams: Processes, Risk, and Mitigation', number 3 in 'ASCE Geotechnical Special Publication', American Society of Civil Engineers, pp. 131–145.

Takahashi, T. (1991), *Debris Flow*, Balkema, Rotterdam.

Takahashi, T. (2007), *Debris Flow: Mechanics, Prediction and Countermeasures*, Taylor Francis Ltd, London.

Takahashi, T. and Kuang, S. (1988), 'Hydrograph prediction of debris flow due to failure of landslide dam', *Annual Report of Disaster Prevention Research Institute, Kyoto University* **31**(B-2), 601–615. In Japanese with English abstract.

Takahashi, T. and Nakagawa, H. (1993), Estimation of flood/debris flow caused by overtopping of a landslide dam, in 'Proceedings of the 25th IAHR World Congress', Vol. III, Tokyo, pp. 117–124.

Takayama, S., Miyata, S., Fujimoto, M. and Satofuka, Y. (2021), 'Numerical simulation method for predicting a flood hydrograph due to progressive failure of a landslide dam', *Landslides* **18**, 3655–3670.

URL: <https://doi.org/10.1007/s10346-021-01712-7>

Van Tien, P., Sassa, K., Takara, K., Fukuoka, H., Dang, K., Shibasaki, T., Ha, N. D., Setiawan, H. and Loi, D. H. (2018), 'Formation process of two massive dams following rainfall-induced deep-seated rapid landslide failures in the kii peninsula of japan', *Landslides* **15**, 1761–1778.

URL: <https://doi.org/10.1007/s10346-018-0988-y>

Wada, T., Nakatani, K., Satofuka, Y., Mizuyama, T., Kosugi, K. and Miwa, H. (2021), 'Development of a numerical model for deposition and flood propagation by multiple inflows of debris flows and river floods', *International Journal of Erosion Control Engineering* **14**(2), 20–30.

URL: <https://doi.org/10.13101/ijece.14.20>

Walder, J. S. and O'Connor, J. E. (1997), 'Methods for predicting peak discharge of floods caused by failure of natural and constructed earthen dams', *Water Resources Research* **33**(10), 2337–2348.

URL: <https://doi.org/10.1029/97WR01616>

Zhong, Q. M., Chen, L. C., Mei, S. Y., Shan, Y., Wu, H. and Zhao, K. P. (2024), 'Numerical investigation of hydro-morphodynamical characteristics of a cascading failure of landslide dams', *Journal of Mountain Science* **21**(6), 1868–1885.

URL: <https://doi.org/10.1007/s11629-023-8411-0>

Zhong, Q. M., Chen, S. S., Deng, Z. and Mei, S. A. (2019), 'Prediction of overtopping induced breach process of cohesive dams', *Journal of Geotechnical and Geoenvironmental Engineering* **145**(5), 04019012.

URL: [https://doi.org/10.1061/\(ASCE\)GT.1943-5606.0002035](https://doi.org/10.1061/(ASCE)GT.1943-5606.0002035)

Zhou, G. G. D., Zhou, M., Shrestha, M. S., Song, D., Choi, C. E., Cui, K. F. E., Peng, M., Shi, Z., Zhu, X. and Chen, H. (2019), 'Experimental investigation on the longitudinal evolution of landslide dam breaching and outburst floods', *Geomorphology* **334**, 29–43.

URL: <https://doi.org/10.1016/j.geomorph.2019.02.035>